Physica Scripta. Vol. T35, 226–231, 1991.

Magneto-Quantum Transport in 2D-Electron Systems with Periodic Modulation

Dieter Weiss

Max-Planck-Institut für Festkörperforschung, Heisenbergstr.1, D-7000 Stuttgart 80, Germany

Received March 18, 1990; accepted November 18, 1990

Abstract

The low temperature magnetoresistance of a high mobility two-dimensional electron gas – realized in GaAs–AlGaAs heterojunctions – is dominated by Shubnikov–de Haas oscillations, reflecting the discrete nature of the electron energy spectrum. When a weak one- or two-dimensional periodic potential with period a smaller than the electron mean free path is superimposed on the two-dimensional electron gas a novel type of oscillation occurs which reflects the commensurability of the relevant lengths in these systems – the cyclotron orbit diameter at the Fermi energy and the period a of the periodic potential. Theoretically, this lateral superlattice effect is shown to result from an oscillatory dependence of the bandwidth of the modulation-broadened Landau levels on the band index.

1. Introduction

Modern lithographic techniques allow the investigation of electron transport in systems where the relevant lengths (elastic mean free path, phase coherence length, magnetic length, Fermi-wavelength) are comparable with the sample size. A variety of novel effects have been observed in such mesoscopic systems [1]. Such techniques can also be used to superimpose an artificial periodic potential on a two-dimensional electron gas (2-DEG). The motion of conduction electrons under the combined influence of a magnetic field and a periodic potential has been extensively studied both theoretically and experimentally (see e.g., [2–5] and references therein). Such systems have quite recently attracted some interest, since the superimposed periodic potential leads to a novel type of magnetoresistance oscillation periodic in $1/B$, as long as the period of the modulation is small compared to the mean free path of the electrons [6]. The periodicity of these oscillations is governed by an interesting commensurability problem owing to the presence of two length scales, the period a of the potential and the cyclotron radius R_C at the Fermi energy [6, 7]. We have used the persistent photoconductivity effect – a characteristic feature of GaAs–AlGaAs heterostructures [8] – to create one-and two-dimensional periodic potentials in the submicrometer range. A spatially modulated photon flux results in a spatially modulated positive background charge in the Si-doped AlGaAs layer which in turn leads to a periodic potential in which the electrons have to move. In our measurements a holographic illumination of the heterostructure at liquid helium temperatures is used to produce a periodic potential, a method first used by Tsubaki *et al.* [9]. We produce only a weak periodic potential: the modulation obtained by this technique is on the order of 1 meV where the Fermi energy E_F in our samples is typically 10 meV. Without periodic modulation one obtains the well known parabolic energy dispersion characteristic for a 2-DEG and the contour of constant energy at E_F is a circle with radius k_F. Switching on a weak magnetic field would force the electrons to move around this Fermi circle, corresponding also to a circular motion in real space. The effect of a superimposed one-dimensional (1D) periodic potential in x-direction, e.g., with period a is that it opens up gaps at the new Brillouin zone boundaries at multiples of $\pm\pi/a$. The existence of gaps at the Bragg planes leads to open orbits in k_x-direction which implies an electron motion in y-direction in real space. This additional conductivity in y-direction is known to give a positive magnetoresistance ρ_{xx} [10] in the x-direction. Increasing the magnetic field increases the probability for an electron to tunnel through the classically forbidden region and performing now a circular motion. This effect is known as magnetic breakdown [11]. Under this condition the positive magnetoresistance saturates since the electrons now behave as in a homogeneous 2-DEG. At higher magnetic fields the Landau level (LL) quantization must be taken into account. Since we have a weak periodic potential only the gaps between the lowest bands will be significant [12]. For a typical period of 300 nm and a carrier density $N_S = 2 \times 10^{11}\,\mathrm{cm}^{-2}$ we note that we have about 10 bands occupied corresponding to 20 Bragg planes intersecting the original Fermi circle. Therefore we do not expect a significant influence of the periodic potential on the transport properties at zero magnetic field since the Fermi energy is located high in the bandstructure where the dispersion is almost that of a free 2-DEG. The situation changes, however, when a magnetic field is switched on. This will be shown in the next section, where the experiments displaying the novel magnetoresistance oscillations are briefly reviewed.

2. Magnetoresistance oscillations

The experiments were carried out using conventional AlGaAs–GaAs heterostructures grown by molecular beam epitaxy with carrier densities between $1.5 \times 10^{11}\,\mathrm{cm}^{-2}$ and $4.3 \times 10^{11}\,\mathrm{cm}^{-2}$ and low temperature mobilities ranging from $0.23 \times 10^6\,\mathrm{cm}^2/\mathrm{Vs}$ to $1 \times 10^6\,\mathrm{cm}^2/\mathrm{Vs}$. Illumination of the samples increases both the carrier density and the mobility at low temperatures. The electron mean free path l_e ($= v_F\tau$) in our samples can therefore be as high as 15 μm. We use an L-shaped geometry to investigate the magnetotransport properties parallel and perpendicular to the 1D-periodic potential. Some of the samples investigated have an evaporated semi-transparent NiCr front gate. A sketch of the experiment using the persistent photoconductivity to periodically modulate the positive background charge in the AlGaAs-layer is shown in Fig. 1(a) and 1(b). We use either a HeNe laser ($\lambda = 633$ nm) or an Argon–Ion laser ($\lambda = 488$ nm). The expanded laser beam enters the sampleholder through a quartz window and a shutter. Two mirrors mounted close to

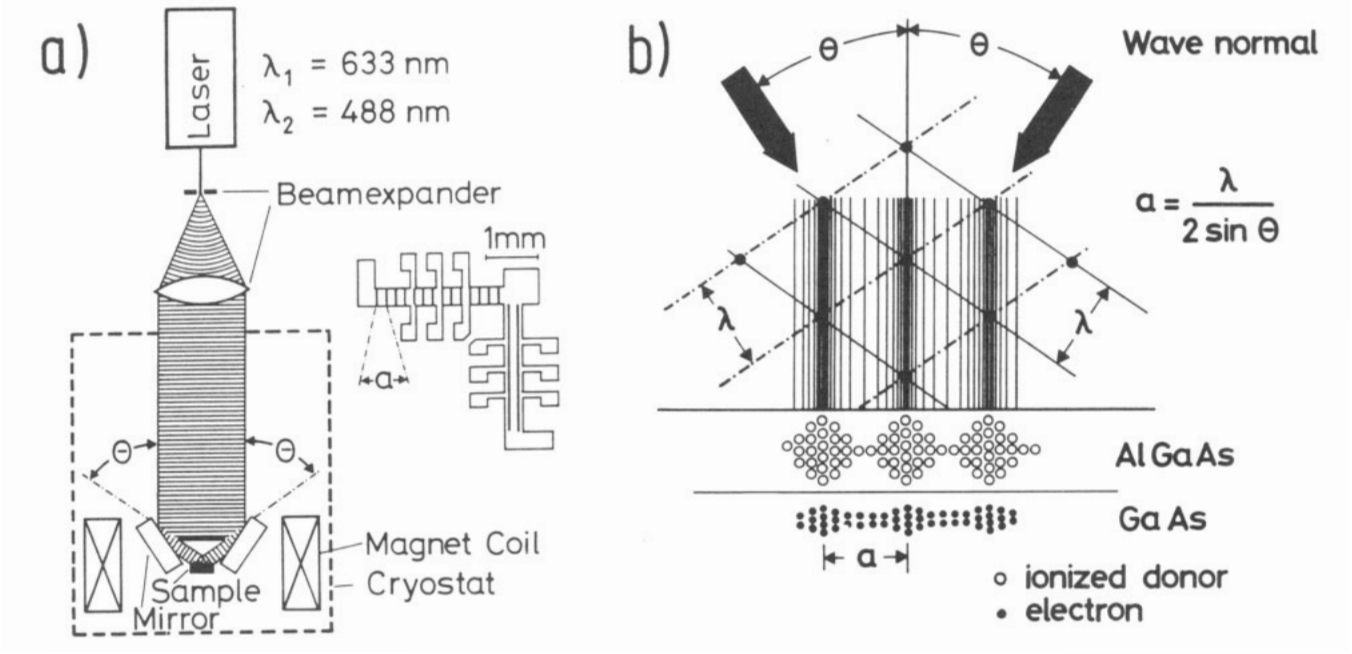

Fig. 1. (a) Schematic experimental set up (left hand side) and top view of the L shaped sample geometry where the interference pattern is sketched. (b) Sketch of the spatial modulation of the concentration of ionized donors in the AlGaAs layer and of electrons in the 2-DEG produced by holographic illumination using two interfering laser beams with wavelength λ. The interference pattern created is shown schematically.

the sample are used to create two interfering plane light waves. The advantage of this kind of "microstructure engineering" is its simplicity and the achieved high mobility of the microstructured sample due to the absence of defects introduced by the usual pattern transfer techniques [1].

The result of standard magnetoresistance measurements carried out perpendicular ($\rho_\perp = \rho_{xx}$) and parallel ($\rho_\parallel = \rho_{yy}$) to the periodic modulation is shown in Fig. 2. In addition to the usual Shubnikov–de Haas (SdH) oscillations appearing at about 0.5 T additional oscillations become visible at even lower magnetic fields. While pronounced oscillations of this new type dominate $\rho_\perp$ at low magnetic fields, weaker oscillations with a phase shift of 180° relative to the $\rho_\perp$ data are visible in the $\rho_\parallel$ measurements. No additional structure appears in the Hall resistance. The novel oscillations are, analogous to SdH oscillations, periodic in $1/B$ as is displayed in the inset of Fig. 2. The periodicity is given by the commensurability condition

$$2R_c = (\lambda - \tfrac{1}{4})a, \qquad \lambda = 1, 2, 3, \ldots, \tag{1}$$

between the cyclotron diameter at the Fermi level, $2R_c = 2v_F/\omega_c = 2l^2 k_F$, and the period a of the modulation. Here $k_F = \sqrt{2\pi N_s}$ is the Fermi number, $l = \sqrt{\hbar/eB}$ the magnetic length, and $\omega_c = \hbar/m^* l^2$ the cyclotron frequency with the effective mass $m^* = 0.067\, m_0$ of GaAs. For magnetic field values satisfying eq. (1) minima are observed in $\rho_\perp$. The validity of eq. (1) has been confirmed by performing these experiments on different samples, by changing the carrier density with an applied gate voltage, and by using two laser wavelengths in order to vary the period a [6]. To resolve an oscillation an elastic mean free path l_e at least as long as the perimeter of the cyclotron orbit is required. This agrees with our finding that the number of oscillation periods resolved depends on the mobility of the sample: the higher the mobility the more oscillations are observable since the electrons can traverse more periods of the potential ballistically. Consistent experimental results have been obtained by Winkler *et al.* [13] and Alves *et al.* [14] using conventionally microstructured samples.

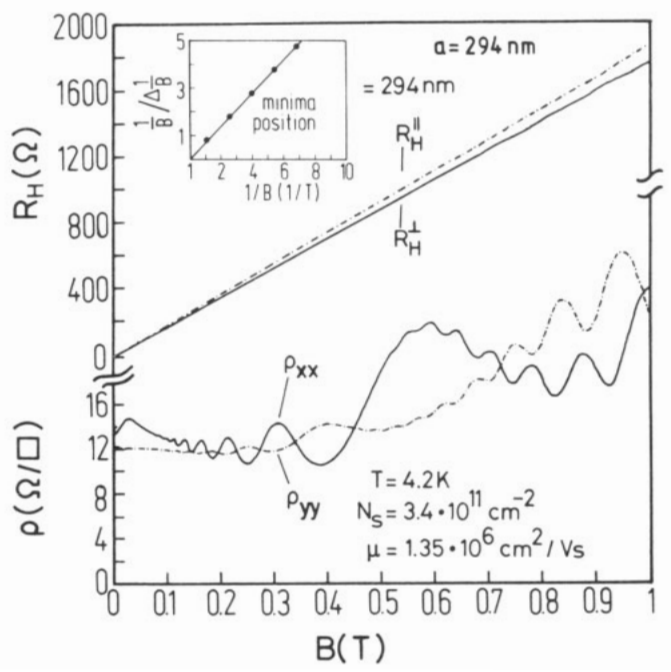

Fig. 2. Magnetoresistivity ρ and Hall resistance R_H parallel and perpendicular to the interference fringes. The positions of the minima of $\rho_\perp$ are plotted in the inset demonstrating the $1/B$ periodicity of the novel oscillations.

3. Origin of the oscillations

The common origin of both types of oscillations is a modification of the Landau level energy spectrum. This has been pointed out by Gerhardts *et al.* [7] and Winkler *et al.* [13] who attributed the $\rho_\perp$ oscillations to an additional band conductivity discussed in Section 3.2. However, there are other models explaining the $\rho_\perp$ oscillations. Beenakker [15] noticed that these oscillations can be attributed to a "guiding center

drift resonance". He showed for high temperatures that it is not necessary to start from the LL energy spectrum and to treat the problem quantum-mechanically. In this limit the oscillations in $\rho_\perp$ can be explained semiclassically. Quite recently Streda and MacDonald [16] explained the oscillations by an oscillating probability for magnetic breakdown. However, all the theories above cannot explain the oscillations in $\rho_\parallel$. One has to go beyond the constant scattering time approximation as first pointed out by Gerhardts [12].

3.1. *Landau levels in a 1D-periodic potential*

The energy spectrum of electrons subjected to both a magnetic field and a periodic one-dimensional potential has been calculated by several authors [17–19] using first order perturbation theory. Starting point is a Hamiltonian of the form

$$H = \frac{1}{2m^*}\left[-\hbar^2\frac{\partial^2}{\partial x^2} + \left(\frac{\hbar}{\mathrm{i}}\frac{\partial}{\partial y} + \frac{e}{c}Bx\right)^2\right] + V_0\cos(Kx) \tag{2}$$

containing a periodic potential in x-direction $V(x) = V_0\cos(Kx)$ with period $a = 2\pi/K$. The energy spectrum can be taken in first order perturbation theory in V and is given by:

$$E_n(x_0) \approx (n + \tfrac{1}{2})\hbar\omega_c + \langle nx_0|V(x)|nx_0\rangle. \tag{3}$$

The right hand side matrix element (containing the harmonic oscillator wavefunctions $|nx_0\rangle$ of the homogeneous 2-DEG) can be regarded as effective potential acting on an electron averaged over the spatial extent of the wavefunction $|nx_0\rangle$ given by $2l\sqrt{2n+1}$ which is equal to the classical cyclotron diameter $2R_c$ for high quantum numbers n. Two special situations can be considered as is sketched in the upper half of Fig. 3. Assuming, for the sake of simplicity, a stepfunction like wavefunction, the matrix element $\langle nx_0|V(x)|nx_0\rangle$ at the Fermi energy vanishes if the cyclotron diameter equals an integer of the period a leading to a flat Landau band, independent of the center coordinate x_0. On the other hand, a maximum of the matrix element is expected for a cyclotron diameter equal to an odd integer of half the period a leading to Landau bands with strong curvature with respect to x_0. More precisely, the matrix element $\langle nx_0|V(x)|nx_0\rangle$ can be calculated analytically giving

$$E_n(x_0) \approx (n + \tfrac{1}{2})\hbar\omega_c + U_n\cos Kx_0 \tag{4}$$

with $U_n = V_0\exp(-\frac{1}{2}X)L_n(X)$ where $X = \frac{1}{2}K^2l^2$ and $L_n(X)$ stands for the n-th Laguerre polynomial. $L_n(X)$ is an oscillating function of both its index n and its argument X where the flat band situation is given by $L_n(X) = 0$. This flat band condition can be expressed in terms of the cyclotron radius R_c and is given by eq. (1) [7]. A typical energy spectrum – calculated in first order perturbation theory – is plotted in Fig. 3. The corresponding density of states (DOS) is sketched on the right hand side in Fig. 3. The existence of the shape of the DOS sketched in Fig. 3 can be directly proven by magnetocapacitance experiments as has been shown recently [20, 21]. The modified energy spectrum sketched in Fig. 3 is the key for the explanation of the periodic potential induced oscillations given in the next section.

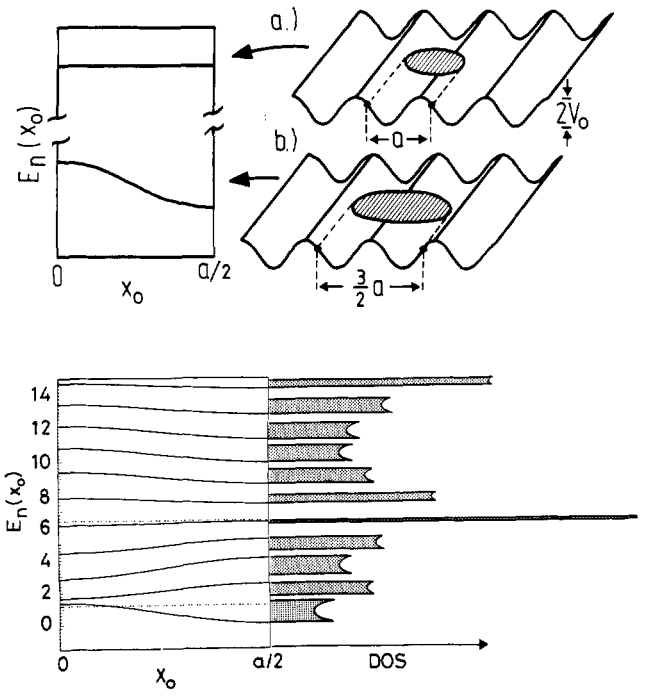

Fig. 3. Simplified picture explaining the oscillating Landau level width (upper part) and calculated energy spectrum (in meV, first order perturbation theory) for for $B = 0.8$ T, $V_0 = 1.5$ meV and $a = 100$ nm. The corresponding DOS is sketched. The dashed lines correspond to the flat band situation determined by eq. (1).

3.2. *Oscillations in $\rho_\perp$: Additional bandconductivity*

The theory presented here follows closely the calculations of Gerhardts *et al.* [7] for a cosine modulation in x-direction. The oscillations in $\rho_\perp$ $(=\rho_{xx})$ can be understood within a simple damping theory which means that electron scattering is described by a constant relaxation time τ. The k_y dispersion of the Landau energy spectrum leads to an additional contribution to the conductivity σ_{yy} which is within the framework of Kubo's formula (see e.g., Ref. [22]) given by

$$\Delta\sigma_{yy} = \frac{2e^2\hbar}{2\pi l^2}\int_0^a\frac{\mathrm{d}x_0}{a}\sum_n\left(-\frac{1}{\gamma}\frac{\mathrm{d}f}{\mathrm{d}E}(E_n(x_0))|\langle nx_0|v_y|nx_0\rangle|^2\right) \tag{5}$$

where $\gamma = \hbar/\tau$, f is the Fermi function, $|nx_0\rangle$ are the eigenstates of eq. (2) and v_y is the velocity operator in the y direction. These eigenstates carry current in the y direction

$$\langle nx_0|v_y|nx_0\rangle = -\frac{1}{m^*\omega_c}\frac{\mathrm{d}E_n}{\mathrm{d}x_0} = \frac{1}{\hbar}\frac{\mathrm{d}E_n}{\mathrm{d}k_y} \tag{6}$$

but not in the x-direction,

$$\langle nx_0|v_x|nx_0\rangle = 0, \tag{7}$$

which is the reason for the anisotropic behaviour of σ_{xx} and σ_{yy}. Note that conductivity and resistivity in a magnetic field are connected by $\rho_{xx} = \sigma_{yy}/D$ and $\rho_{yy} = \sigma_{xx}/D$ and $D = \sigma_{xy}^2 + \sigma_{xx}\sigma_{yy}$ (see e.g., [23]). For high magnetic fields $(\omega_c\tau \gg 1)\,\sigma_{xy} \gg \sigma_{xx}\sigma_{yy}$ holds. In eq. (6) the modified energy spectrum comes into play. The matrix element $\langle x_0n|v_y|x_0n\rangle$ vanishes always when flat Landau bands (see e.g., Fig. 3) are located at the Fermi energy and $\Delta\sigma_{yy} = 0$. Consequently $\Delta\rho_{xx}$ (the extra contribution to the resistivity ρ_{xx}) also vanishes. On the other hand $\mathrm{d}E_n/\mathrm{d}x_0$ displays a maximum value when the Fermi energy is located within the Landau band with the strongest dispersion and therefore $\Delta\sigma_{yy}$ $(\Delta\rho_{xx})$ is at maximum. A calculation based on the evaluation of eq. (5) which

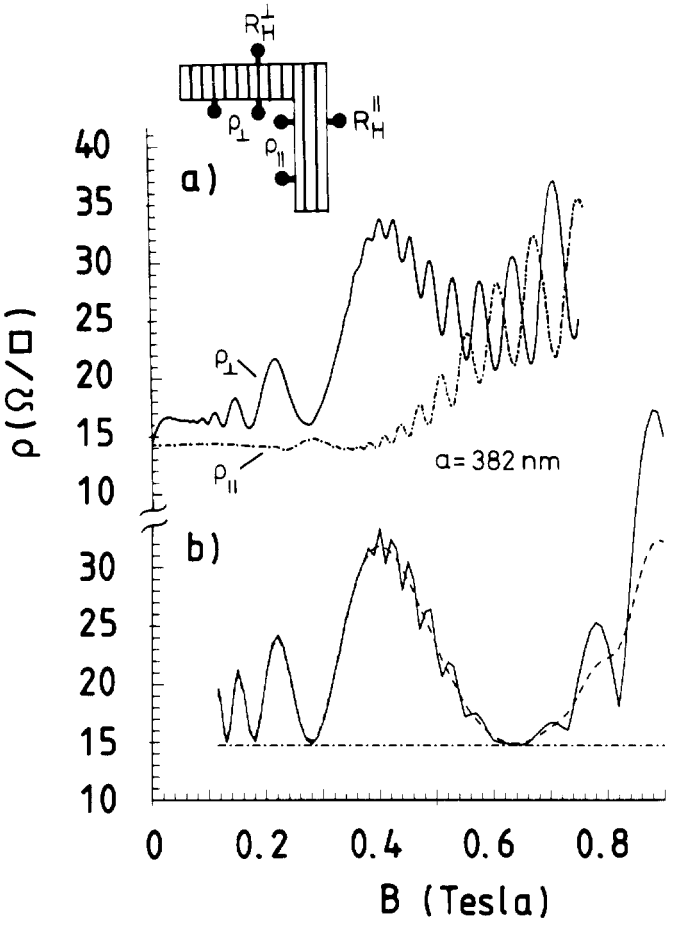

Fig. 4. Magnetoresistivities for current perpendicular and parallel to the interference fringes for a sample with $N_S = 3.16 \times 10^{11}\,\mathrm{cm}^{-2}$, and $\mu = 1.3 \times 10^6\,\mathrm{cm}^2/\mathrm{Vs}$ (a) measured at temperature $T = 2.2\,\mathrm{K}$; (b) calculated for $T = 2.2\,\mathrm{K}$ (solid line) and for 4.2 K (dashed line) [7].

is compared to experimental magnetoresistivity data is shown in Fig. 4. The experiment is nicely reproduced assuming a modulation potential of 0.3 meV in the calculations (solid lines in Fig. 4). In the high temperature limit ($\hbar\omega_c < kT$) and for high quantum numbers n the expression for the additional conductivity becomes much simpler [13] and can be expressed making use of the fact that $\Delta\rho_{xx} \approx \Delta\sigma_{yy}/\sigma_{xy}^2$:

$$\Delta\rho_{xx} \approx \frac{1}{2\pi\hbar}\frac{V_0^2}{\gamma\hbar\omega_c}\frac{4}{ak_F}\frac{B^2}{N_s^2}\cos^2\left(2\pi\frac{R_c}{a}-\frac{\pi}{4}\right). \tag{8}$$

Equation (8) may be used to estimate from the amplitudes $\Delta\rho_{xx}^{max}$ of the commensurability oscillations the amplitude V_0 of the superimposed periodic potential. From the maximum of ρ_{xx} at 0.41 T (Fig. 4(a)) one estimates $V_0 = 0.28\,\mathrm{meV}$ in good agreement with the calculation in Fig. 4b.

While the low field oscillations of ρ_{xx} are nicely reproduced by the calculation, the calculated ρ_{yy}-data (dashed-dotted line in Fig. 4(b)) display simply the magnetic field independent Drude result in contrast to the experiment which shows maxima when the Landau bands are flat (corresponding to a high DOS at E_F). This is not too surprising since one cannot describe the usual SdH oscillations of a homogeneous 2-DEG within the constant relaxation time approximation; one ends up with the simple Drude result. The same result has been obtained by Beenakker using his semiclassical model [15].

3.3. *Oscillations in $\rho_\parallel$: Oscillating scattering rate*

The results in the previous section have been obtained using the constant scattering time approximation which, however, has no justification. For a homogeneous electron gas in a quantizing magnetic field it is well known that the scattering time itself depends on the DOS [24]. In order to understand the experimentally observed ρ_{yy} ($=\rho_\parallel$) oscillations one has to go beyond this approximation — in analogy to the description of the SdH oscillations — and consider a density-of-states-dependent scattering rate. In the calculations one has to go through the formalism of the selfconsistent Born approximation [24] using the solutions of eq. (2). A detailed description of this theory has been given by Zhang and Gerhardts [25]. In analogy to the theory of SdH oscillations they find that

$$\sigma_{xx} \propto D_T^2(\mu) = \int \mathrm{d}E \frac{\mathrm{d}f(E-\mu)}{\mathrm{d}\mu} D(E)^2 \tag{9}$$

where $D_T^2(\mu)$ is the thermal average of the square of the DOS. It should be emphasized that even for $kT \approx \hbar\omega_c$ where the individual LL's are no longer resolved in ρ_{yy}, $D_T^2(\mu)$ oscillates, reflecting the oscillating DOS sketched in Fig. 3. Consequently one can observe low field oscillations in ρ_{yy} even when in this magnetic field range no SdH oscillations are resolvable [26]. From eq (9) it follows that the weak antiphase oscillations in ρ_{yy} are in phase with the density of states oscillations and maxima in ρ_{yy} are always observed when the DOS at the Fermi-energy is at maximum, in contrast to ρ_{xx} which displays minima when the Landau bands are flat since $\mathrm{d}E_n/\mathrm{d}x_0 = 0$. This behaviour is in agreement with the experiment displayed in Fig. 2. Recent calculations by Vasilopoulos and Peeters [27] show similar results but with much smaller amplitude of the ρ_{yy} oscillations.

4. Positive low field magnetoresistance and magnetic breakdown

The low field oscillations in $\rho_\perp$ are accompanied by a positive low field magnetoresistance which saturates below 0.2 T. This positive magnetoresistance is absent in $\rho_\parallel$ as is displayed in Fig. 2. Applying a negative gate voltage on the semi-transparent top gate one can increase the built in periodic modulation amplitude V_0 [28] which results in turn in an increased positive magnetoresistance step shown in Fig. 5. Such a behaviour would be expected for magnetic breakdown, mentioned in the introduction. Open orbits in k_x direction (see inset of Fig. 6) give an additional contribution to σ_{yy} and lead to a positive magnetoresistance in ρ_{xx} [10] as long as the electrons can move in open orbits. The probability p for an electron to tunnel from an open orbit (a) to a circular orbit (b) in Fig. 6 is given in the literature by $p = \exp(-B_0/B)$ with the magnetic breakdown field B_0:

$$B_0 = \frac{\pi m^* E_g^2}{4e\hbar E_F \sin 2\Theta} \tag{10}$$

where E_g is the energy gap at the Brillouin zone boundary and Θ the angle defined by $\cos\Theta = \pi/ak_F$ [29]. For sufficiently weak periodic potentials we may assume — following Streda and MacDonald [16] — that gaps $E_g \approx V_0$ exist only at the boundary of the *first* Brillouin zone. Using eq. (8) we can extract V_0 from the low field ρ_{xx} oscillations in Fig. 5 and

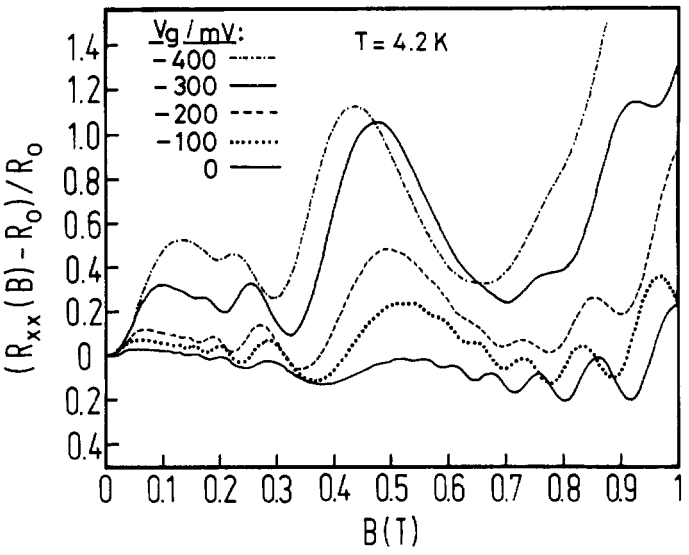

Fig. 5. Normalized magnetoresistance for different gate voltages. With increasing negative bias, both, the amplitude of the low field oscillations and the magnetic field value where the positive magnetoresistance disappears (taken as B_0) increases.

compare the calculated B_0 values with those taken from the experiment (the magnetic field where the positive magnetoresistance saturates). The comparison is plotted in Fig. 6. The calculated B_0 values are not in perfect agreement with the experimental ones. For higher modulation amplitudes V_0, eq. (10) overestimates the breakdown field B_0. One should bear in mind, however, that we do not take into account finite temperature effects and the existence of higher gaps.

5. Magnetoresistance in a two-dimensional periodic potential

In this last section results of low field magnetotransport experiments in a two-dimensional periodic potential are presented. In such a potential grid the commensurability problem becomes more severe as compared to the 1D case and results in a complicated energy spectrum [2–5]. In a weak

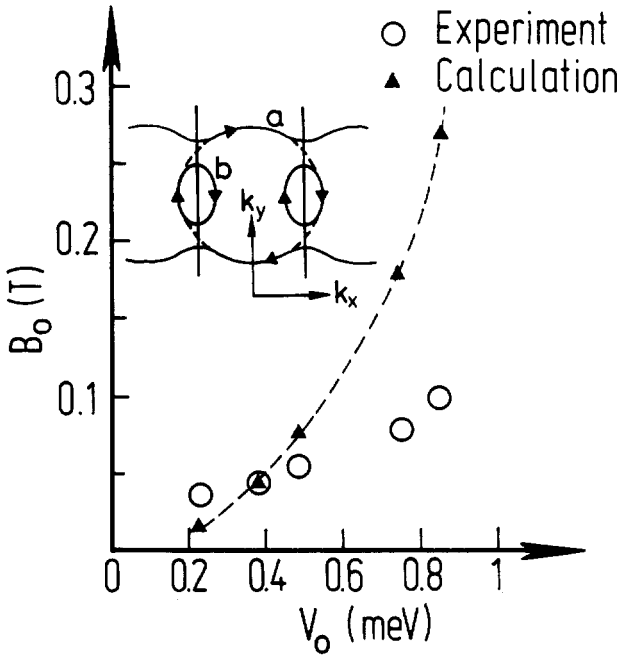

Fig. 6. Comparison of calculated (eq. (10)) and measured (Fig. 5) breakdown fields B_0. The inset shows the contours of constant energy at E_F for a weakly modulated 2-DEG in the extended zone scheme.

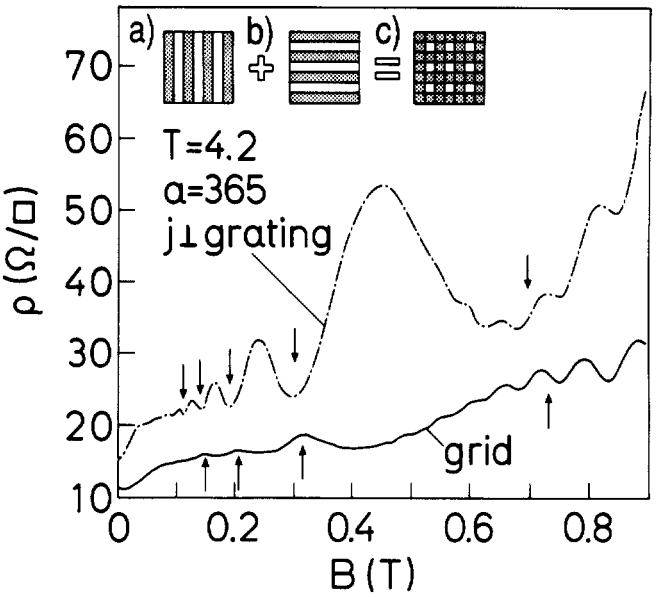

Fig. 7. Magnetoresistance in a grating (current ⊥ grating) and grid. The creation of the holographically defined pattern is shown schematically. The arrows correspond to eq. (1).

2D-periodic potential the LL spectrum depends on the flux $\Phi = Ba^2$ penetrating one unit cell. If $\Phi/\Phi_0 = q/p$ where Φ_0 is the flux quantum and p/q is a rational number, the 2D-periodic potential splits one LL into q subbands separated by gaps (see e.g., [5]). The LL width, on the other hand, is modulated by Laguerre polynominals very similar to the 1D case (eq. (4)), so that the flat band condition for 1D- and 2D-periodic potentials is the same [30]. This has also been demonstrated experimentally [14, 21, 28]. In our experiments the two-dimensional periodic potential ($V_0 \ll E_F$) with $a = 365$ nm is created by successive holographic illumination of a high mobility GaAs–AlGaAs heterostructure ($\mu = 1.2 \times 10^6 \text{cm}^2/\text{Vs}$ corresponding to $l_e = 10\,\mu\text{m}$). Holographic illumination of type (a) in Fig. 7 produces additional oscillations in the magnetoresistance due to an additional bandconductivity (dashed-dotted line in Fig. 7). An additional holographic illumination where the sample has been rotated by 90° results then in a grid potential sketched in Fig. 7(c). The magnetoresistance obtained under such conditions (solid line in Fig. 7) displays a weak oscillating behaviour also corresponding to the commensurability condition eq. (1), with maxima where ρ_{xx}-measured for situations (a)-shows minima. If one starts with an illumination of type (b) followed by (a) one ends up with the same result. Therefore one can conclude that the 2D-periodic potential destroys the bandconductivity oscillations triggered by $\langle nx_0|v_y|nx_0\rangle \propto dE_n/dk_y$ for the 1D case. If the collision broadening for the 2D case is small compared to the gaps between the LL subbands the corresponding matrix elements are significantly reduced so suppressing the bandconductivity contributions [30]. Since this seems to be the case in our experiments we can only observe the scattering rate oscillations displaying maxima when the flat band condition eq. (1) is fulfilled. This experiment provides indirect evidence for the existence of gaps inside an LL due to the 2D-periodic potential.

Acknowlegements

I would like to thank K. von Klitzing, R. R. Gerhardts, C. Zhang, U. Wulf, G. Müller and D. Heitmann for valuable discussions and I am grateful to

K. Ploog and G. Weimann for providing me with high quality samples. I also would like to thank P. Streda and A. MacDonald for making [16] available to us prior to publication.

References

1. For recent work in this field see Physics and Technology of Submicron Structures (Edited by H. Heinrich, G. Bauer and F. Kuchar), Springer Series Solid-State Sciences **83**, (1988); Nanostructure Physics and Fabrication (Edited by M. Reed and W. P. Kirk), Academic Press (1989).
2. Harper, P. G., Proc. Phys. Soc. **A68**, 874 (1955).
3. Azbel, M. Y., Sov. Phys.-JETP **19**, 634 (1964).
4. Hofstadter, D. R., Phys. Rev. **B14**, 2239 (1976).
5. Thouless, D. J., in The Quantum Hall Effect (Edited by R. E. Prange and S. M. Girvin), Springer (1987).
6. Weiss, D., v. Klitzing, K., Ploog, K. and Weimann, G., Europhys. Lett. **8**, 179 (1989); also in The Application of High Magnetic Fields in Semiconductor Physics (Edited by G. Landwehr), Springer Series in Solid-State Sciences **83**, (1989).
7. Gerhardts, R.R., Weiss, D. and v. Klitzing, K., Phys. Rev. Lett. **62**, 1173 (1989).
8. Störmer, H. L., Dingle, P., Gossard, A. C., Wiegmann, W. and Sturge, M. D., Solid State Commun. **29**, 705 (1979); Schubert, E. F., Knecht, J. and Ploog, K., J. Phys. **C18**, L215 (1985).
9. Tsubaki, K., Sakaki, H., Yoshino, J. and Sekiguchi, Y., Appl. Phys. Lett. **45**, 663 (1984).
10. Ashcroft, N. W. and Mermin, N. D., Solid State Physics, Hott, Rinehart and Winston (1976).
11. Cohen, M. H. and Falicov, L. M., Phys. Rev. Lett. **7**, 231 (1961).
12. Gerhardts, R. R., in "Science and Engineering of 1- and 0-Dimensional Semiconductors" (Edited by S. P. Beaumont and C. M. Sotomayor Torres), (Plenum, London 1990).
13. Winkler, R. W., Kotthaus, J. P. and Ploog, K., Phys. Rev. Lett. **62**, 1177 (1989).
14. Alves, E. S., Beton, P. H., Henini, M., Eaves, L., Main, P. C., Hughes, O. H., Toombs, G. A., Beaumont, S. P. and Wilkinson, C. D. W., J. Phys. **C1**, 8257 (1989).
15. Beenakker, C. W. J., Phys. Rev. Lett. **62**, 2020 (1989).
16. Streda, P. and MacDonald, A. H., Phys. Ref. **B41**, 11892 (1990).
17. Aizin, G. R. and Volkov, V. A., Sov. Phys. JETP **60**, 844 (1984) [Zh. Eksp. Teor. Fiz **87**, 1469 (1984)].
18. Kelly, H. J., J. Phys. **C18**, 6341 (1985).
19. Chaplik, A. V., Solid State Commun. **53**, 539 (1985).
20. Weiss, D., Zhang, C., Gerhardts, R. R., von Klitzing, K. and Weimann, G., Phys. Rev. **B39**, 13030 (1989).
21. Ismail, K., Smith, T. P. III and Masselink, W. T., Appl. Phys. Lett. **55**, 2766 (1989).
22. Kubo, R., Miyake, S. J. and Hashitsume, N., Solid State Physics **17**, 239 (1965); Gerhardts, R. R., Z. Physik **B21**, 285 (1975).
23. Pippard, A. B., Magnetoresistance in Metals (Edited by A. M. Goldman, P. V. E. McClintock and M. Springfield), Cambridge Studies in Low Temp. Physics (1989).
24. Ando, T. and Uemura, Y., J. Phys. Soc. Jpn. **36**, 959 (1974).
25. Zhang, C. and Gerhardts, R. R., Phys. Rev. **B41**, 12850 (1990).
26. Gerhardts, R. R., Zhang, C., Proc. Eighth Intern. Conf. Electronic Properties of Two-Dimensional Systems, Grenoble, France 4–8 Sept. 1989, Surf Sci. **229**, 92 (1990).
27. Vasilopoulos, P. and Peeters, F. M., Phys. Rev. Lett. **63**, 2120 (1989).
28. Weiss, D., von Klitzing, K., Ploog, K. and Weimann, G., Proc. Eighth Intern. Conf. Electronic Properties of Two-Dimensional Systems, Grenoble, France 4–8 Sept. (1989), Surf. Sci. **229**, 88 (1990).
29. Blount, E. I., Phys. Rev. **126**, 1636 (1962); Pippard, A. B., Proc. Roy. Soc. (London) A, **270**, 1 (1962); Reitz, J. R., J. Phys. Chem. Solids **25**, 53 (1964).
30. Gerhardts, R. R., Weiss, D. and Wulf, U., Phys. Rev. **B43**, to appear.